

# Nomadic Planets Near the Solar System

T. Marshall Eubanks<sup>1</sup> \*

<sup>1</sup>Asteroid Initiatives LLC, Clifton, Virginia, USA

in original form 13 November 2014

## ABSTRACT

Gravitational microlensing has revealed an extensive population of “nomadic” planets not orbiting any star, with Jupiter-mass nomads being more populous than main sequence stars. Except for distant objects discovered through microlensing, and hot, young nomads found near star formation regions, to date only a small number of nomad candidates have been discovered. Here I show that there should be significant numbers of mature nomadic exoplanets close enough to be discovered with existing or planned astronomical resources, including possibly dozens of massive planets closer than the nearest star. Observational data are used to derive models relating mass, radius, heat flux and magnetic dipole moment; these are used to show the observability of nomads in the IR, due to thermal emissions, and at radio frequencies, due to cyclotron maser instabilities. These neighboring nomadic planets will provide a new exoplanet population for astronomical research and, eventually, direct exploration by spacecraft.

**Key words:** planets and satellites: detection – infrared: planetary systems – radio continuum: planetary systems – brown dwarfs

## 1 INTRODUCTION

Although the concept of nomadic exoplanets<sup>1</sup> (also called rogue planets) has a fairly long history (Öpik 1964; Fogg 1990), they were only firmly detected relatively recently. Nomadic planets young enough to remain hot ( $\gtrsim 1000$  K) are likely to be found near the site of their formation, and the first nomads were found in star formation regions as a result of near-InfraRed (near-IR) searches (Zapatero Osorio et al. 2000). Gravitational microlensing is in principle well suited for the discovery of a galactic population of older, colder, nomads, but the expected duration of lensing events in the galactic bulge is  $\sim 1.5 \sqrt{M/M_{Jupiter}}$  days for a lens of mass M, and early microlensing surveys of bulge stars did not have a sufficiently high cadence to reliably detect the brief events expected from Jupiter-mass nomads. Mature (cool) nomadic planets were thus only firmly detected in the 2006-2007 microlensing data from the MOA-II survey, with cadences of 10 to 50 min (Sumi et al. 2011). These microlensing observations show that nomadic Jupiter-mass planets are more common than main sequence stars, implying a population of nomads closer than the nearest stars. A few nomads have recently been discovered relatively near the Sun, but they are mostly fairly young and warm objects (Delorme et al. 2012; Howard et al. 2014). A very recent discovery (Luhman 2014b), WISE J085510.83-071442.5 (or W0855), is the coldest known brown dwarf or exoplanet, with an effective

temperature of 235–260 K and a parallax distance of only  $7.58 \pm 0.26$  ly (Luhman & Esplin 2014), is a candidate member of the set of neighboring nomadic exoplanets discussed in this paper.

Sumi et al. (2011) used microlensing data to estimate the ratio of the number density of Jupiter-mass unbound exoplanets,  $n_J$ , and the number density of main sequence stars  $n_*$ , yielding an estimate  $n_J / n_* = 1.9^{+1.3}_{-0.8}$  for their power law model. The stellar number density is well known from luminosity data (Chabrier 2001), yielding an estimate for  $n_J$ ,

$$n_J = (6.7^{+6.4}_{-3.0}) \times 10^{-3} \text{ ly}^{-3} \quad (1)$$

and thus an estimate for the expected mean distance to the nearest Jupiter mass nomadic planet,  $D_J$ , with

$$D_J = 3.28^{+0.7}_{-0.6} \text{ ly} , \quad (2)$$

the mean minimum distance being  $\sim 77\%$  of the distance to Proxima Centauri.

While the nearest nomadic planets will be close enough for intensive study, they should also sample conditions of

<sup>1</sup> This paper defines a nomadic planet, or nomad, as any exoplanet not bound to a star, an exoplanet as any condensed normal matter object outside the solar system with a mass, M,  $\geq$  the Lunar mass,  $M_{Moon}$  and  $\leq$  the deuterium burning limit of 13 times the mass of Jupiter,  $M_{Jupiter}$ , and a brown dwarf as any such object with a mass such that  $13 M_{Jupiter} < M \leq 65 M_{Jupiter}$ , the hydrogen burning limit.

planetary formation throughout the galaxy. Recent work shows that stars migrate throughout the Galaxy after their formation (Roškar 2013); nearby nomadic planets can similarly be expected to participate in widespread migrations and thus come from throughout the galaxy. The nearby nomadic planets will also sample the varieties of planetary evolution. Nomads could be “native,” forming outside any star system, or “stellar,” ejected from their birth stellar system by a variety of mechanisms, including by scattering during planetary formation, by scattering or galactic tides during their host star’s main sequence phase, or by being shed as a result of stellar mass loss after the end of their host’s main sequence (Veras et al. 2013). The primary sources of nomadic planets remain unclear, but as planet-planet scattering and post-main sequence shedding certainly should produce nomads but even together are apparently insufficient to explain the observed nomadic number density (Veras & Raymond 2012), there is likely to be a significant population of both stellar and native nomads close to the solar system.

The population density of the nomad exoplanets is sufficiently large (see Section 2) that there are good prospects of discovering at least the more massive close bodies (roughly of the mass of Saturn or larger) through observation of either their IR thermal (Sections 3 and 4) or their radio maser-cyclotron emissions (Sections 5 and 6). As is discussed in Section 7, while discovering neighboring nomads through microlensing is unlikely with current technology, due to the very low optical depth and brief durations expected for these events, the post-discovery prediction and observation of microlensing events by nearby nomads should play an important role in their study, by providing a means for the direct determinations of their masses. Finally, Section 8 describes how the close nomadic planets, despite their cold exteriors, could be possible locations for both active and fossil biologies, and thus are likely to provide the closest objects of astrobiological interest outside of our own solar system.

## 2 THE NUMBER DENSITY OF NOMADIC EXOPLANETS

The number density model used in this paper is combination of two power laws (Sumi et al. 2011; Strigari et al. 2012), with the nomadic planet (nm) model being

$$\frac{dn_{nm}}{dM} = \kappa_{nm} M^{-\alpha_{nm}}, \quad (3)$$

where  $n_{nm}$  is the number density (in units of  $\text{ly}^{-3}$ ) for a planet of mass  $M$ ,  $\kappa_{nm}$  is a constant, set by the number of Jupiter mass nomads, and  $\alpha_{nm}$  the power law exponent. A similar equation, with different numerical values, is used for the brown dwarf (bd) density. This and subsequent calculations assume that nomadic planets and brown dwarfs are distributed randomly in space (following a 3-dimensional Poisson distribution), that their number density does not depend on location in the Galactic disk, and that the combined number density is continuous at  $13 M_{Jupiter}$ . I also assume the “Jupiter-mass object” number ratio of Equation 1 corresponds to a number density integral about a decade in mass logarithmically centered on  $1 M_{Jupiter}$  (i.e., an integral over  $M_{Jupiter}/\sqrt{10} \leq M < \sqrt{10} M_{Jupiter}$ ); plots and estimates in this paper based on object number densities are

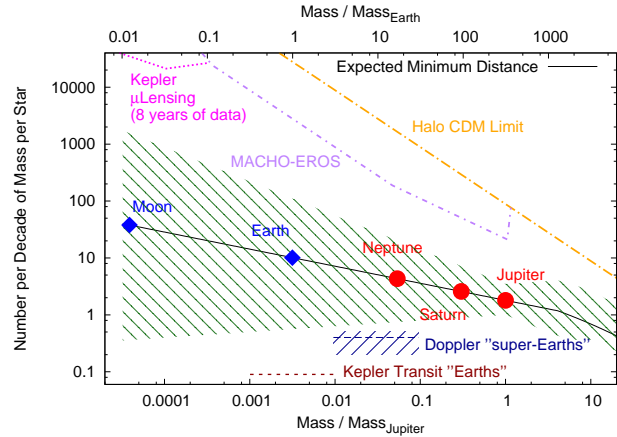


**Figure 1.** The nomadic planet number density per decade of mass compared to the total galactic stellar density. The two lower curves are estimates of the fraction of stars with an orbiting Earth or super-Earth, while the upper curves are upper bounds of the number density, from Galactic kinematics (the Halo CDM limit) and from gravitational microlensing from the ground-based MACHO-EROS surveys. The Kepler microlensing limit are actually a prediction of the limit possible with a nominal 8 year mission. (The mean values for the objects with the masses of solar system objects are shown here and in Figure 2 as a convenience to the reader.)

unless otherwise stated likewise are based on integrals over a decade in mass centered on the reporting value. (Note that for  $M > 4.1 M_{Jupiter}$  estimates averaged over a decade in mass include a contribution from the brown dwarf distribution.)

The Sumi et al. (2011) estimate for the power law exponents are

$$\alpha_{mn} = 1.3^{+0.3}_{-0.4}. \quad (4)$$

for the nomadic planets and

$$\alpha_{bd} = 0.48^{+0.24}_{-0.27}. \quad (5)$$

for the brown dwarfs. A strong anticorrelation was reported (Strigari et al. 2012) between the estimates of  $\alpha_{mn}$  and  $\alpha_{bd}$ ; this was assumed to be  $= -1$  in calculating errors. The scale of the brown dwarf distribution is set by the finding (Kirkpatrick et al. 2012) that the total number of hydrogen-burning stars outnumber brown dwarfs by a factor of  $\sim 6$ . Equations 3 and 4 were applied between the mass of the Moon ( $4 \times 10^{-5} M_{Jupiter}$ ) and the Deuterium burning limit ( $\sim 13 M_{Jupiter}$ ), with the brown dwarf power law extending the number density model up to  $65 M_{Jupiter}$ .

Figure 1 shows the integrated number density for the entire nomadic planet mass range, relative to the total main sequence number density, together with the error derived from the quoted formal errors (displayed as the right-sloping cross-hatching). Independent upper bounds of the number density of compact objects of any sort are provided by the additional curves above the number density estimate in Figure 1. The Halo Cold Dark Matter (CDM) curve is derived assuming that the entire Galactic Halo dark matter density, as estimated using stellar kinematics (Bovy & Tremaine 2012), is due to compact objects of the given mass, while the MACHO+EROS constraints are from ground-based op-

tical microlensing observations (Alcock et al. 1998). These independent gravitational lensing constraints indicate that there cannot be more than  $\sim 1000$  Earth-mass nomads per star, and thus that  $\alpha_{nm}$  is  $\lesssim 2.2$ .

The two horizontal lines below the hatched number density curve are estimates of the density of exoplanets in stellar orbits, from Kepler transit discoveries of Earth-mass planets (the lower dashed line) (Lissauer, Dawson & Tremaine 2014) and ground based radial velocity discoveries of super-Earths for  $M \sin i = 3$  to 30 times the mass of the Earth,  $M_{Earth}$ , where  $i$  is the unknown inclination of the Doppler-discovered exoplanet (slightly above and to the right of the Kepler estimate) (Mayor, Lovis & Santos 2014). These estimates surprisingly appear to indicate that Earths and super-Earths are more likely to be nomads than in stellar orbits; more probably this simply reflects observational biases due to the difficulty of discovering small planets and planets with long orbital periods.

Figure 2 shows the expected minimum distance,  $R_{min}$ , as a function of nomad mass. The nearest “dark-Jupiter” should be considerably closer than Proxima Centauri, and there should thus be a few Jupiter-mass nomads within the distance to that star. The expected minimum distances of brown dwarfs are, by comparison, considerably larger, and it appears statistically unlikely that there are many (if any) brown dwarfs closer than the recently discovered Luhman 16 binary (Luhman 2013). Luhman (2014a) used WISE space telescope data to bound the minimum distance to solar companions with the mass of Jupiter and Saturn. These limits would also apply to mature nomadic planets of roughly the solar age and are consistent with the expected minimum distances to those bodies.

In order to predict the number densities of nomadic exoplanets with masses much smaller than that of Jupiter it is necessary to extrapolate the power law models into mass regimes not yet well constrained by microlensing (Strigari et al. 2012), leading to the three order of magnitude uncertainty in the number density of Earth-mass nomads in Figure 1 and the factor of almost 6 uncertainty in the distance to the nearest Earth-mass nomad seen in Figure 2. This uncertainty is driven by the uncertainty in  $\alpha_{nm}$ , which is sufficiently large that it is not certain whether the the nomadic planet number distribution is dominated by the smallest or the largest bodies, i.e., whether  $\alpha_{nm} > 1$ , as is the case for stars and for the larger Kuiper Belt Objects (Strigari et al. 2012), or is  $\leq 1$ , as is the case for Brown Dwarfs, with  $\alpha_{bd} \sim 1/2$ . This uncertainty in  $\alpha_{nm}$  considerably inflates the uncertainty in the numbers of smaller nomadic planets, such as for the Earth-mass nomads. One way to resolve this uncertainty would be to extend the gravitational lensing detection of nomadic exoplanets to lower masses, ideally down to lenses with the mass of the Earth or smaller.

An Earth-mass gravitational lensing event in the galactic bulge would have a typical duration of  $\sim 2$  hours; microlensing surveys with cadences of minutes are thus required to significantly bound the galactic population of Earth-mass nomads with gravitational lensing. The Kepler space telescope survey for transiting planets has a cadence of 30 minutes; these data usefully limit the microlensing rate of Halo MACHO objects in the mass range from  $\sim 0.002$  to  $\sim 0.1 M_{Earth}$  (Griest, Cieplak & Lehner 2013). Kepler, however, only observes  $\sim 150,000$  stars at one time, and these

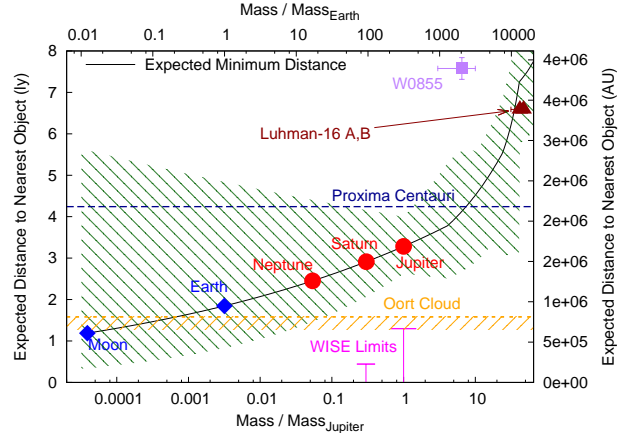


**Figure 2.** The expected minimum distance,  $R_{min}$ , as a function of nomadic planets mass, based on the power law number-density models derived from observations. The estimated limit of the solar system’s Oort cloud of comets is shown, along with the distance to Proxima Centauri, as horizontal lines. The estimated distance and masses for the closest known brown dwarfs, the Luhman 16 binary, are also shown; these agree well with the predicted closest distances for those masses. By contrast, W0855, the cold nomadic planet WISE J085510.83-071442.5, is considerably more distant than the predicted closest distance for its mass, and so it would be reasonable to expect there would be closer nomads of similar masses. The “WISE Limits” are for mature nomadic planets (or solar companions) with the mass of Jupiter and Saturn, respectively (see text).

stars are closer than the bulge stars typically used in microlensing surveys, which lowers the expected optical depth for nomadic planet lensing, with the result that even a full 8 years of mission data (see Figure 1) would not be sufficient to significantly bound the population density predicted for Earth-mass nomadic planets (Cieplak & Griest 2013). Improved constraints on the number density of Earth-mass nomads will require either dedicated ground based surveys (Jung et al. 2014) or the implementation of some of the proposed space-based microlensing surveys (Beaulieu, Tisserand & Batista 2013).

### 3 THERMAL MODELING OF NOMADIC PLANETS

Nearby nomadic planets are likely to have the same age range as nearby stars, from  $\lesssim 1$  Gyr to as old as the Galactic disk itself ( $8.8 \pm 1.7$  Gyr) (del Peloso et al. 2005; Vican 2012); nearby nomadic Halo planets could be even older. The models in this paper are intended to be conservative estimates of thermal radiation for mature nomadic exoplanets of roughly the age of the solar system. Fortney et al. (2011) used radiative-convective models of Jupiter, Saturn, Uranus and Neptune to estimate the change in the thermal luminosities of these bodies with time. While younger planets of the same mass could be significantly more luminous, and thus easier to detect, than the solar system giants, these more detailed models indicate that the decline in luminosity for giant planets older than the solar system is likely to be relatively small, less, in calculating the observabilities of the

closest giant planet nomads, than the uncertainties in their likely distances.

Mature nomads should be close to radiative equilibrium on their surfaces or upper cloud-tops, and in the black body approximation used here will radiate according to their size and internal heating. Previously derived models derived from exoplanet data are used to estimate planetary radii as a function of mass (subsection 3.1), while solar system data are used to derive power density models (subsection 3.2), thus enabling the estimation of the IR flux of mature nomads as a function of mass.

### 3.1 Planetary Mass-Radius Relations

It is possible to estimate both the planetary mass and radius for some well-observed exoplanets (primarily those with both stellar transits and Doppler radial velocity data); the recent proliferation of such data has thus substantially improved knowledge of planetary radii as a function of mass, particularly for masses between the Earth and Neptune, and those larger than Jupiter, where there are no solar system analogues. Figure 3 shows the mass-radius relation for every exoplanet in the exoplanet.eu database (Schneider et al. 2011) as of October 4, 2014, together with similar data for the solar system planets, the Moon, Titan and the Galilean satellites, and also for three well-studied radio-loud Ultra-Cool brown Dwarfs (UCDs) (see Nichols et al. 2012, and Section 5). There are different mass-radius relations for terrestrial planets and giant planets, and both these planetary types display an apparent change in their equation of state for sufficiently large masses (Chabrier et al. 2009).

This paper uses the models of Marcy et al. (2014) for “terrestrial” planets (tp), those with masses roughly between  $M_{Moon}$  and  $30 M_{Earth}$ . There is an apparent change in the mass-radius relation at  $R \sim 1.5 R_{Earth}$  (or  $M \sim 4 M_{Earth}$ ); below that size, the density typically increases with mass, while above that size the radius is roughly  $\propto$  mass, and the bulk density thus decreases with mass (Marcy et al. 2014). The decreasing density is thought to reflect the presence of an extended Hydrogen-Helium atmosphere for the larger bodies (Mordasini et al. 2012). The Marcy et al. radius and density models for terrestrial planets are

$$\begin{aligned} \rho_{tp} &= 2320 + 3190 \frac{R}{R_{Earth}} \text{ kg m}^{-3} & M \leq 4 M_{Earth} \\ \frac{R}{R_{Earth}} &= 0.345 \times \frac{M}{M_{Earth}} & M > 4 M_{Earth} \end{aligned} \quad (6)$$

These models are based on exoplanet data up to  $\sim 4 R_{Earth}$  (or  $\sim 10 M_{Earth}$ ); the terrestrial radius model for masses  $> 30 M_{Earth}$  (indicated by the dotted line in Figure 3) is both an extrapolation and matches none of the available data, and so is not used.

Objects with roughly the solar composition and a mass between  $\sim 1$  and  $\sim 80 M_{Jupiter}$ , which includes Jupiter and super-Jupiter mass exoplanets together with brown dwarfs and even some low mass stars, have radii close to that of Jupiter, but with a slight decline with increasing mass (Chabrier et al. 2009). This paper uses the mass-radius relationship for gas giants (gg) derived using CoRoT space telescope data (Hatzes 2014), with

$$\rho_{gg} = \begin{cases} 730 & \text{kg m}^{-3} & M \leq M_{Jupiter} \\ 730 \times \left( \frac{M}{M_{Jupiter}} \right)^{1.17} & \text{kg m}^{-3} & M > M_{Jupiter} \end{cases} \quad (7)$$

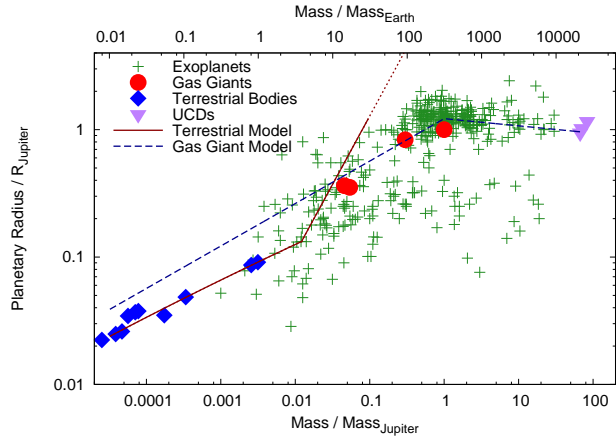


**Figure 3.** The planetary and UCD radius as a function of mass, for the Moon, Titan, the Galilean satellites and the 8 planets of the solar system, the 1822 exoplanets in the exoplanet.eu database as of October 4, 2014, and 3 fast rotating UCDs. The terrestrial radius model is based on exoplanet data up to  $\sim 10 M_{Earth}$ ; in this paper the terrestrial radius model for masses  $> 30 M_{Earth}$  (indicated by the dotted line) is assumed to be unreliable and is not used.

This curve is the dashed line in Figure 3; the transition from the constant density was chosen to begin at  $1 M_{Jupiter}$  to improve the fit to the giant planets in the solar system. Note that many of the discovered exoplanets are hot Jupiters orbiting close to their stars; these objects seem to be slightly inflated (with radii  $\sim 10\%-25\%$  greater than predicted in Equation 7), and thus appear above this curve in Figure 3.

### 3.2 Thermal Power Generation as a Function of Mass

The study of the solar system indicates that the internal heating of mature exoplanets should be dominated by energy from long-lived radioactive elements (for terrestrial planets) or from the settling of denser components towards the body’s core (for the gas giants). Given the limited amount of solar system data on internal planetary heating, and a near total absence of relevant exoplanet data, very simple models were derived assuming that internal power generation is proportional to mass for the two different planet types. (It is likely that there are other planetary types, but hopefully the two solar system types span a reasonable fraction of the actual nomadic planets.) With these models, it is straightforward to compute the black body intensity as a function of wavelength for a planet of a given mass and type, and then estimate the maximum distance this could be detected for a given telescope sensitivity, and to use the estimated number density to determine the probability of finding one or more such bodies within that distance.

Estimation of a planet’s black body thermal emission requires an estimate of its radius (subsection 3.1) and internal heating. Figure 4 shows determinations of the internal energy production for bodies in the solar system, based on direct estimates of heat flow for the Earth (Davies & Davies 2010) and Moon (Siegler & Smrekar 2014), and astronomical and spacecraft observations of excess heat production for Jupiter (Li et al. 2012), Saturn (Hanel et al. 1983; Li

et al. 2010), Uranus (Stier et al. 1978; Pearl et al. 1990) and Neptune (Stier et al. 1978; Pearl & Conrath 1991). (Heat flow estimates are also available for the Galilean satellites, but these are dominated by Jovian tidal heating.)

There appear to be at least two different regimes of internal power density, with the Earth and Moon producing nearly the same power per unit mass, and Jupiter and Saturn also having similar, but considerably larger, power densities (see Figure 4). A very simple model for power density,  $\varpi$ , for the two planet types is thus based on the average for each pair, with

$$\varpi = \begin{cases} 7.9 \times 10^{-12} \text{ W kg}^{-1} & \text{terrestrial planets} \\ 1.9 \times 10^{-10} \text{ W kg}^{-1} & \text{gas giants} \end{cases} \quad (8)$$

The power density models are shown as solid and dashed lines in Figure 4; it is assumed in this paper that these two models bound internal power densities of nomadic planets with ages comparable to the solar system. Given an estimate for  $\varpi$ , the black body equilibrium temperatures for nomadic planets can be estimated using the Stefan-Boltzmann law and the radius and power density models of Equations 6, 7 and 8. These models imply substantial differences between the external temperatures of super-Earths and super-Jupiters, with the former decreasing, and the latter, increasing, with mass as shown in Figure 5. The effective surface temperatures of super-Jupiters increase strongly with mass, due to their relatively constant radii, which would move their peak emissions from the far-IR to the mid-IR for the largest nomads. By contrast, the exterior temperature of super-Earths would decrease with mass, due to their decreasing bulk densities. It is worth nothing, as is discussed further in Section 8, that the actual surfaces of the nomadic super-Earths, beneath their thick atmospheres, would increase with mass, and could be warm enough for sufficiently massive bodies to support oceans of liquid water.

It is of course likely that this model will be inadequate in some cases, particularly for exoplanets with masses  $\gg M_{Jupiter}$  (as their power densities will be extrapolated from those of Jupiter and Saturn). In addition, although the two ice giants, Uranus and Neptune, have very similar gross physical characteristics, their internal power estimates differ by at least an order of magnitude; it is interesting that the Voyager derived estimate for the energy density of Uranus (Pearl et al. 1990) is quite close to the that predicted by the terrestrial model for its mass. Finally, note that the use of black-body radiation models does not account for atmospheric spectral features which can be expected to cause a higher or lower luminosity at the wavelengths of various spectral lines.

#### 4 DETECTING NEARBY NOMADIC PLANETS IN THE THERMAL INFRARED

Figure 6 displays the black body flux density expected from a set of hypothetical planets, matching the Earth, Neptune, Saturn and Jupiter in mass, radius and power density, but assumed to be placed at the mean closest distance for a body of that mass. A super-Jupiter with 10 times the mass of Jupiter is also included; that planet's size and power density are given by the gas giant models. Table 1 provides the corresponding numerical results for these bodies. Figure 6

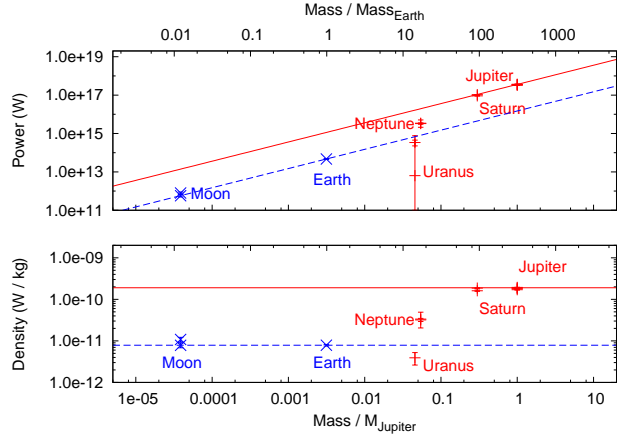


**Figure 4.** Internal power generation as a function of mass for total power (top) together with the power density per unit mass (bottom). The Earth and the Moon have roughly the same power density (W/kg), as do Jupiter and Saturn, but the two gas giants produce substantially more power per unit mass than do the terrestrial bodies. As a simple empirical model, terrestrial planets are assumed to share the Earth-Moon power density, while Jovian planets are assumed to share the Jupiter-Saturn power density. Note that Uranus and Neptune, although superficially similar, have considerably different power densities and do not fit either model well.

also shows flux density limits for actual (ALMA (Baudry 2008), cooled WISE (Wright et al. 2010) and cooled Spitzer (Barlow 2012) and planned (SPICA (Onaka et al. 2004) and JWST (Barlow 2012) telescopes and arrays. All of the solar system analogues would have peak flux density in the Far-IR, while the super-Jupiter radiation would peak in the mid-IR. The super-Jupiter and Jupiter analogs would be detected by five of the instruments, the Saturn analog by four, while the Neptune and Earth analogs would not be detected by any of them.

Similar insights can be obtained by investigating the flux density as a function of mass for the observing frequencies of various instrumental channels. Figures 7, 8 and 9 show black body flux density estimates as a function of mass at 675 GHz (440 μm), 70 μm and 18 μm, representative channels of ALMA, SPICA and JWST, respectively. Despite the different wavelengths and instruments, all of these provide a somewhat similar conclusion : it should be possible to detect the closest giants down to or somewhat below the mass of Jupiter, but terrestrial nomads are unlikely to be discovered with current technology. Table 1 shows that Jupiter mass nomads could be detected out to ~10 ly by SPICA or JWST, implying that a few dozens could be discoverable, while possibly hundreds of super-Jupiters could be discovered within a range of a few dozens of ly by the JWST at 10 μm.

It thus seems likely that if a nearby gas giant nomad is discovered, by whatever means, it would be possible to study it by observations of its thermal emissions over a wide range of wavelengths. Unfortunately, neither SPICA nor the JWST is intended as a full sky survey instrument; the discovery of the majority of the nearest nomadic gas giants in the IR would probably require a suitable far-IR survey telescope, for which there are apparently no plans at present.

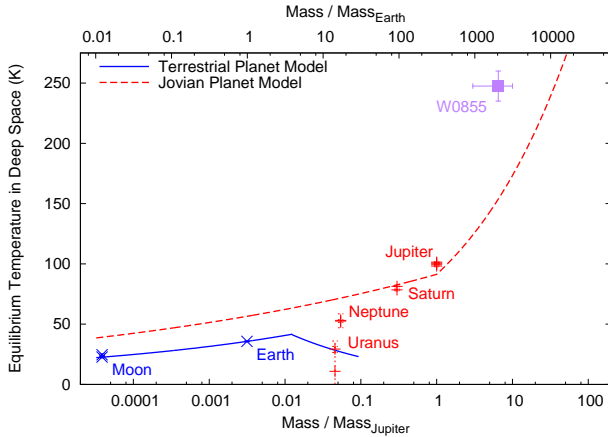


**Figure 5.** The equilibrium temperature in deep space due to internal power generation for mature planets far from any significant external energy sources. The terrestrial planet temperature model assumes a density implied by Equation 6; the Giant planet model assumes the densities implied by Equation 7. The values for the various solar system planets are those implied by their actual mass, radius and internal power generation. W0855 (WISE J085510.83-071442.5) is a recently discovered nomadic planet. Although it is the coldest nomad known at present, these models indicate that it is warmer than would be expected for a solar system analog. It is thus presumably either still fairly young, or the models are overly conservative for super-Jupiters.

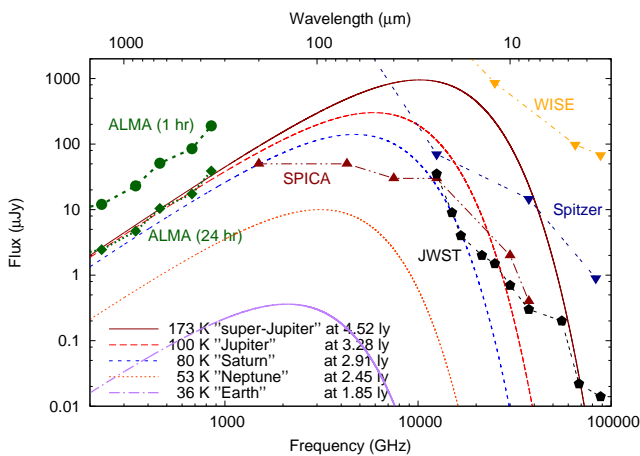


**Figure 6.** The IR flux density for black bodies with the same radius and internal power generation as the actual Earth, Neptune, Saturn and Jupiter (see Figure 4), plus a model-derived “super-Jupiter” with a mass of  $10 M_{Jupiter}$ , each with the temperature of a black body and the mean closest distance for a nomadic body of that mass (i.e., the central curve in Figure 2), together with flux density limits for various actual (ALMA, cooled Spitzer, cooled-WISE) and planned (SPICA and JWST) telescopes and arrays. (The lines connecting the various channels for the different instruments are only to guide the eye.)

Fortunately, it may be possible to discover a substantial fraction of these bodies through their non-thermal radio emissions.

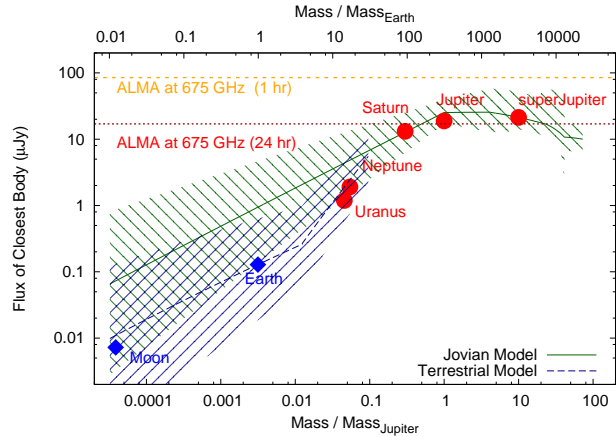


**Figure 7.** The flux density of the closest nomadic exoplanet as a function of mass for the 675 GHz ( $440 \mu m$ ) channel of the ALMA array. While short duration (1 hour) ALMA integrations are unlikely to detect nomadic exoplanets, longer (24 hour) integrations should be able to detect the closest nomadic gas with masses greater than Saturn, but not substantially less massive objects. (In this and Figures 8 and 9, the displayed flux densities for solar system objects are based on their actual internal heat generation and radius, while the flux densities for the  $10 M_{Jupiter}$  super-Jupiter is based purely on the gas giant model.)

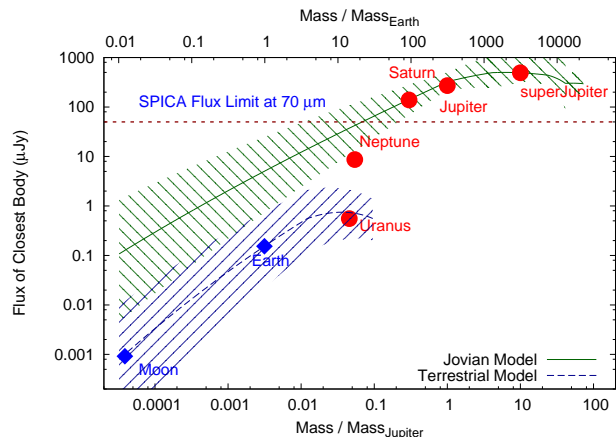


**Figure 8.** The flux density of the closest nomadic exoplanet as a function of mass at  $70 \mu m$ , compared with the estimated sensitivity of the  $70 \mu m$  channel of the proposed SPICA space telescope (this limit is a confusion limit, not a bare flux density limit). The estimated sensitivity of SPICA at this wavelength should be able to detect the closest nomadic giant planets, but would not be able to detect nearby nomadic “super-Earths,” at least at their expected distances.

## 5 CYCLOTRON MASER RADIO EMISSIONS FROM NOMADIC EXOPLANETS

A completely different means of discovering magnetized nomadic planets is by searching for non-thermal radio emissions generated by the electron Cyclotron Maser Instability (CMI). The strongly magnetized bodies in the solar system (the Earth plus the 4 giant planets) are all strong non-thermal radio emitters, with the decametric emissions from Jupiter at times having a greater luminosity than the Sun in the range 10–40 MHz (the so-called “High Frequency,”

[p]

**Table 1.** Minimum expected distances from the best-fit microlensing population densities for analogues for solar system planets (plus a  $10 M_{Jupiter}$  “super-Jupiter”), together with the surface temperature, wavelength of peak flux density, the flux density at the spectral peak, and the detection range of the SPICA  $70 \mu m$ . For the analogs of solar system bodies the black body model uses the actual radius and the measured internal power generated; for the super-Jupiter the radius, temperature and thermal power are entirely based on the gas giant model.

Object Analog	Mass	Expected $R_{min}$	Peak $\lambda$	flux density at Peak and $R_{min}$	Detection Limit	
	$M_{Jupiter}$	ly	$\mu m$	$\mu Jy$	SPICA @ $70 \mu m$	JWST @ $18 \mu m$
Earth	0.003	$1.85^{+2.99}_{-1.01}$	143	$0.36^{+1.41}_{-0.31}$	0.10	0.001
Neptune	0.054	$2.45^{+1.95}_{-0.99}$	96	$10.0^{+18.0}_{-6.9}$	0.42	0.10
Saturn	0.299	$2.91^{+1.24}_{-0.84}$	64	$140^{+137}_{-71}$	4.83	3.10
Jupiter	1	$3.28^{+0.71}_{-0.65}$	51	$302^{+168}_{-98}$	7.62	9.99
super-Jupiter	10	$4.52^{+1.16}_{-1.61}$	29	$952^{+1357}_{-327}$	14.16	58.17

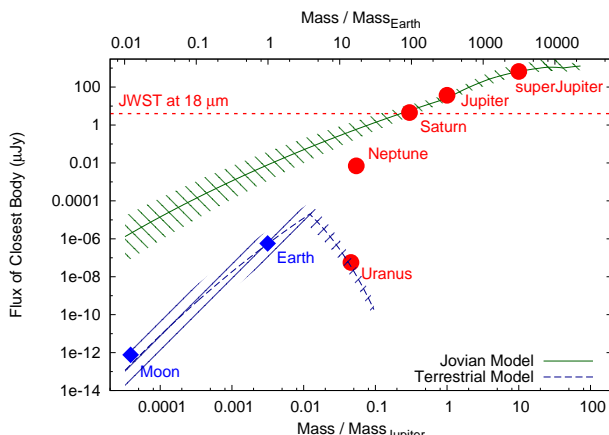


**Figure 9.** The flux density of the closest nomadic exoplanets as a function of mass at  $18 \mu m$ , compared with the estimated sensitivity of the  $18 \mu m$  MIRI channel of the JWST space telescope ( $10 \sigma$  detection with  $10^4$  s integration). The estimated sensitivity of the JWST at this wavelength should be able to detect the closest nomadic gas giants with masses greater than that of Saturn.

or HF, band). The CMI is the primary source of this intense Decametric radiation; these emissions occur from a body moving through a plasma (such as the moon Io orbiting in the rotating Jovian field), with either the body or the plasma, or both, possessing a significant magnetic field (Zarka 1998; Grießmeier, Zarka & Girard 2011; Cecconi et al. 2012), or even from a single, rapidly rotating, magnetized body (Nichols et al. 2012). Such emissions provide a non-thermal means of searching for magnetized exoplanets (Lazio et al. 2004), including magnetized nomads (Vanhämeäki 2011). In the solar system, 5 of the 8 planets (and all of the giant planets) have a magnetic field strong enough to create a “motional” CMI, driven by the blockage of the solar wind by the planetary magnetosphere, while Jupiter (one quarter of the giant planets) produces an even stronger strong “unipolar” CMI radio flux, primarily due to electrons flowing through the Jupiter-Io flux tube. If these occurrence rates are typical for nomadic planets, the search for CMI emissions may provide the best prospects for discovering neighboring nomadic gas giant planets from ground-based observations.

At present non-thermal radio emissions have not been conclusively detected from any exoplanet, stellar or nomadic, but they have been detected from brown dwarfs. In particular, about 6% of the lowest mass brown dwarfs, the so-called “Ultra-Cool Dwarfs” (UCD), (i.e., dwarfs with spectral types of M7 and later) rotate extraordinary rapidly (with periods as low as 2 hours, or  $\sim 5$  times more rapidly than Jupiter), are strongly magnetized and intense sources of circularly polarized CMI radiation, which seems to be driven purely by their rotation. Three of these objects, TVLM 513-46546, 2MASS J00361617+1821104 and LSR J1835+3259, have been studied in detail (Hallinan et al. 2008; Nichols et al. 2012) and are used in this paper as proxies for radio-loud exoplanets. While there are no solar system analogues for the “rotational” CMI of the rapidly rotating UCDs, it seems reasonable to assume that similar emissions can be emitted by rapidly rotating gas giants, and it is possible that a similar percentage of the nomadic Jupiter and super-Jupiter exoplanets produce rotational CMI emissions.

As neither planetary dipole moments nor planetary cyclotron masers can be fully modeled from first principles, scaling relations are used to estimate emissions for arbitrary sized exoplanets (Lazio et al. 2004). Subsection 5.1 derives a double power law model for planetary magnetic moments as a function of mass and rotation period; that model plus the planetary radius is used to estimate the cyclotron frequency,  $f_{cyclotron}$ , as a function of mass, which determines the CMI frequency range. Subsection 5.2 describes the expected motional flux density from the motion of nomadic planets through the ISM, while subsection 5.3 describes a combined model for unipolar and rotational flux densities based on the Jupiter-Io and UCD CMI. It should be recognized that estimates from these empirical scaling relationships are quite uncertain; even the limited data available suggests that they will rarely be significantly more accurate than an order of magnitude.

### 5.1 Double Power Law Models for Magnetic Dipole Moments

Figure 10 shows magnetic dipole estimates for the planets and moons of the solar system (all 8 planets plus the Moon, Io, Europa, and Ganymede), and the 3 well-studied radio-loud UCDs. These radio-loud objects are both more massive

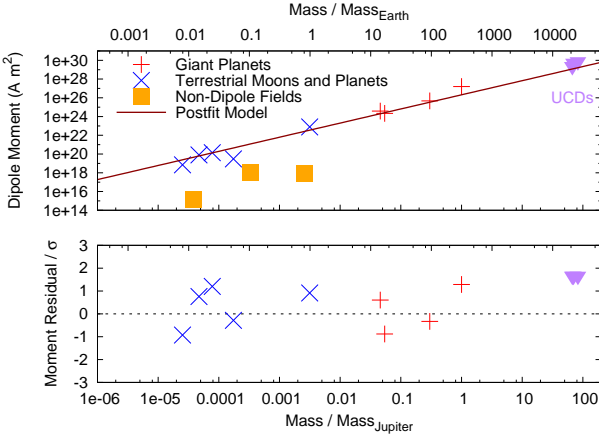


**Figure 10.** The dipole moments for solar system bodies and the three fast UCDs discussed in the text, together with the post-fit power law model of Equation 9 (top) and the residuals from that fit, normalized by the chosen formal errors (bottom). Note that the double power law model includes a scaling with rotation period; the measured rotation frequency is used for the residual calculations for each body, but is set to that of Jupiter’s for the curve marked “postfit model” in the upper plot. The simple double-power law model fits the available dipole data to better than an order of magnitude over a range of 6 orders of magnitude of mass and 3 orders of magnitude of rotation frequency.

and faster rotating than any of the magnetized bodies in the solar system, and help span the exoplanet mass range in the absence of CMI observations of exoplanets. Three bodies (the Moon, Mars and Venus) are displayed as yellow squares. These bodies have weak fields that are not dominated by a dipole component; the dipole moment estimates for these bodies do not fit the model well, were not included in the solution, and are denoted as “non-dipole fields” in this plot.

This paper uses the common double power law model (Durand-Manterola 2009; Vanhamäki 2011) to empirically relate the scalar dipole moment amplitude,  $\mathcal{M}$  to the planet’s mass,  $M$ , and rotation frequency,  $\Omega$ , with

$$\mathcal{M} \sim \mathcal{M}_0 \left( \frac{M}{M_{Jupiter}} \right)^\gamma \left( \frac{\Omega}{\Omega_{Jupiter}} \right)^\varepsilon. \quad (9)$$

The curve in Figure 10, top, is derived from a non-linear least-squares solution for the 3 parameters of this equation using mass, period and dipole moment determinations for 11 bodies, while the bottom figure shows the weighted residuals from the solution. Four bodies were removed from the solution, the three solar system bodies with non-dipole fields plus the UCD LSR J1835+3259, which only has an upper bound for its mass. The solution shown in Figure 10 uses formal errors proportional to the measured dipole moment yielding  $\mathcal{M}_0 = \{3.6 \pm 0.7\} \times 10^{26} \text{ A m}^2$ ,  $\gamma = 1.51 \pm 0.06$  and  $\varepsilon = 0.62 \pm 0.18$ ; both exponents being consistent with the default values (1.5 and 0.75, respectively) used by Vanhamäki (Vanhamäki 2011); the remainder of this paper uses these solve-for values. Since the rotation rate of undiscovered exoplanets is unknown, in calculating properties for nomadic exoplanets I assume for simplicity that each body has the same rotation rate as Jupiter.

The cyclotron frequency,  $f_{cyclotron}$  is a crucial parameter for cyclotron radio observations, as it sets the upper

frequency of the CMI radio emissions. As the Earth’s ionosphere has a lower transmission frequency limit of  $\sim 10$  MHz,  $f_{cyclotron}$  has to be greater than that for ground-based observations to be possible at all. Given the radius and dipole moment,  $f_{cyclotron}$  is given by

$$f_{cyclotron} = \frac{eB_{polar}}{2\pi m_e} \sim \frac{e}{3\pi m_e} \mu_0 \rho \mathcal{M}_0 \left( \frac{M^{\gamma-1}}{M_{Jupiter}^\gamma} \right) \left( \frac{\Omega}{\Omega_{Jupiter}} \right)^\varepsilon \text{ Hz} \quad (10)$$

The  $f_{cyclotron}$  resulting from Equation 10 is shown in Figure 11 (the lower curve), together with estimates (Zarka 1998) of the frequency cutoff of maser cyclotron radiation for the magnetic bodies used in the solution. The full dipole moment solution does a reasonable job of representing the cyclotron frequencies of all the bodies except Jupiter; this is largely due to the model of Equation 9 under-representing the Jovian dipole moment. The upper curve is the “Jovian scaling” of dipole moment equation, where  $\mathcal{M}_0$  is simply set to  $\mathcal{M}_{Jupiter}$ , which seems to provide a more reasonable upper bound for  $f_{cyclotron}$  as a function of mass. Note that even using the full Jovian dipole moment, Jupiter’s apparent cyclotron frequency is still somewhat larger than models predict (Vanhamäki 2011).

Figure 11 shows that even with the Jovian scaling for  $f_{cyclotron}$  only gas giants with  $\sim 0.1 M_{Jupiter} < M < 13 M_{Jupiter}$  would have CMI emissions observable from the surface of the Earth, with the cut-off frequencies for super-Jupiters extending up to  $\sim 150$  MHz (which would make these objects observable with the proposed Square Kilometer Array). UCDs have radii close to that of Jupiter’s and very strong surface fields, up to 0.1 T or more; these bodies thus have cyclotron frequencies of  $\sim 10$  GHz, considerably higher than Jupiter’s, and UCD burst emissions have indeed been detected at frequencies as high as 8.4 GHz (Doyle et al. 2010); simultaneous observations at HF and at GHz wavelengths would help to distinguish between exoplanet and UCD emissions. In the model for terrestrial planets  $f_{cyclotron}$  rapidly declines for masses  $> 4 M_{Earth}$ , as the exoplanet radius becomes roughly  $\propto$  mass. If this decline is realistic, there is little prospect of detecting emissions from terrestrial nomads from the ground, and detection of CMI emissions from nomadic Earths and super-Earths will have to wait for the development of sensitive low-frequency radio instruments in space, such as the arrays proposed (to avoid terrestrial interference) for the far-side or polar regions of the Moon (Jester & Falcke 2009).

## 5.2 Maser Cyclotron Emissions Powered by the InterStellar Medium

The motional emissions in the solar system represent a conversion of the energy of the solar wind into radio power by a planetary magnetosphere, with the power depending on the area of the magnetosphere and the velocity and density of the impinging plasma. The ISM is thought to be nearly stationary in a rest frame moving with the mean galactic rotation, so that the relative velocity,  $\delta V$ , will be dominated by the peculiar velocity of the exoplanet relative to the rotating galactic rest frame. Peculiar velocities of galactic disk objects in the solar neighborhood are of order  $30 \text{ km s}^{-1}$ , while nomadic exoplanets from the galactic halo would have

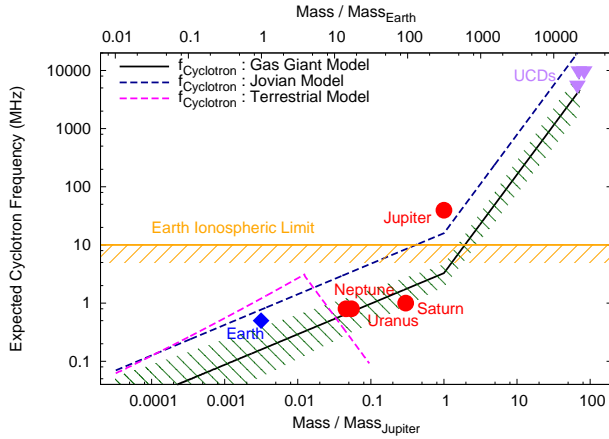


**Figure 11.** Estimated cyclotron frequency as a function of mass, from Equation 10, using the dipole moment scaling of Equation 9, assuming the Jovian rotation period in the dipole moment models. Figure 10 shows that the Jovian dipole moment is underrepresented in the dipole moment model, and the gas giant model cyclotron frequency is thus below the well-determined Jovian cyclotron frequency of  $\sim 39.5$  MHz by a factor of  $\sim 6$ . The “Jovian scaling” uses the same functional form, but scaled to the actual dipole moment of Jupiter for a body with the mass of Jupiter. The UCD data points are lower bounds, as the peak frequency for these bodies has not yet been found.

considerably larger velocities,  $\sim 340$  km s $^{-1}$ , relative to the cold ISM in the galactic disk (Nesti & Salucci 2013). Although the number density of Halo nomadic planets may be much less lower than disk nomads, this higher velocity means that their motion CMI emission would roughly an order of magnitude stronger at a comparable distance. In the absence of good limits for the relative proportions of these two nomad sources, these emissions are bounded in this paper by assuming that all of the nomadic planets are from either the disk or the Halo.

Motional maser cyclotron emissions result from the conversion of the energy in the local medium by the planetary magnetosphere, with a power assumed to be simply related to the size of the planetary magnetosphere,  $R_m$ ,

$$P_{motional} = \beta\pi R_m^2 \delta V p_m \text{ W} \quad (11)$$

where  $\beta$  is a conversion efficiency (Zarka 2010), thought to be of order  $10^{-2}$ , and  $p_m$  is the magnetic pressure of the ISM plasma (Vanhämäki 2011), reasonably thought to dominate over or at least be comparable to the thermal and dynamic pressures, with

$$p_m = \frac{B_{ISM}^2}{2\mu_0} \text{ Pa} , \quad (12)$$

where  $B_{ISM}$ , the external magnetic field strength, is of order  $5 \times 10^{-10}$  T in the “local cloud” of the ISM. The size of the magnetosphere itself depends on a balance of the external and the internal pressure,  $p_{internal}$ , generated by the planetary magnetic field, with

$$p_m = \frac{B_{ISM}^2}{2\mu_0} \sim p_{internal} = \frac{\mu_0 f_0^2 \mathcal{M}^2}{8\pi^2 R_m^6} \text{ Pa} , \quad (13)$$

where  $f_0$  is a form factor thought to be  $\sim 1.16$  (Vanhämäki 2011). Equations 9 and 13 can be used to solve for  $R_m$ , and

thus to determine  $P_{motional}$  for an arbitrary nomadic planet mass,

$$P_{motional} = \beta\delta V \left( \frac{\pi B_{ISM}^4 f_0^2 \mathcal{M}_0^2}{32\mu_0} \right)^{1/3} \times \left( \frac{M}{M_{Jupiter}} \right)^{\frac{2\gamma}{3}} \left( \frac{\Omega}{\Omega_{Jupiter}} \right)^{\frac{2\varepsilon}{3}} \text{ W} \quad (14)$$

This power can be converted into a flux density estimate for a given distance assuming an emission bandwidth (50% of  $f_{cyclotron}$ ) (Vanhämäki 2011) and a beaming factor (1.6 sr) (Nichols et al. 2012).

### 5.3 Unipolar and Rotational Radio Emissions from Nomadic Planets

There is a possibility of strong unipolar CMI emissions from nomadic planets with a suitably large moons inside their magnetospheres (Vanhämäki 2011), and also for rotational CMI emissions for bodies with a sufficiently high rotational frequency (Hallinan et al. 2008). For Jupiter, the Io-related Decametric radiation (Io-DAM) is both stronger and extends to higher frequencies than the Jovian Hectometric Radiation (HOM); the Jupiter Io-DAM are the strongest radio emissions from Jupiter, with an  $\sim 30$  MHz emission bandwidth (Cecconi et al. 2012), a typical power of  $\sim 2 \times 10^{11}$  W, peak power of roughly an order of magnitude higher and very short duration “S-burst” power up to  $\sim 10^{13}$  W at peak (Bose, Sarkar & Bhattacharyya 2008).

Io acts in unipolar CMI as a moving element in a dynamo, with the relative Io-plasma velocity being dominated by the velocity of the rigidly rotating magnetosphere ( $\sim 75$  km s $^{-1}$  at Io), as that is considerably larger than Io’s orbital velocity ( $\sim 17.3$  km s $^{-1}$ ). Io in the Jupiter Io-DAM can thus be treated to a first approximation as a stationary element in a rigidly rotating magnetosphere. In the case of planets or UCDs with rotational CMI, the quasi-rigid rotation of the magnetosphere also seems to be important, and the dynamo effect may be generated in the shear zone where rigid rotation of the magnetosphere breaks down (Nichols et al. 2012). As these objects are much less well understood than the more-accessible solar system CMI emitters, for this paper I will assume that rotational CMI follows the same general scaling relationships as are postulated for unipolar CMI.

Following Vanhamäki (2011), the power generated by a satellite orbiting in the magnetosphere can be estimated by

$$P_{unipolar} = \beta\pi R_{moon}^2 \Delta V \frac{\mu_0 \mathcal{M}^2}{32\pi^2 R_{orbital}^6} \text{ W} \quad (15)$$

where  $R_{moon}$  is the radius of the Moon as sensed by the magnetosphere (as appropriate, either the solid surface or the top of the atmosphere or magnetosphere),  $R_{orbital}$  is the mean radius of the moon’s orbit, and  $\Delta V$  is the difference between the velocity of the magnetosphere and the orbital velocity of the moon. If, as for the Jupiter Io-DAM system, the relative velocity is dominated by the rigid rotation of the magnetosphere,  $\Delta V$  is  $\sim \Omega R_{orbital}$ , with  $\Omega$  being the angular rotation frequency of the primary, so that (using Equation 9)

$$P_{unipolar} \propto R_{moon}^2 \frac{M^{2\gamma} \Omega^{1+2\varepsilon}}{R_{orbital}^5} . \quad (16)$$

$P_{rotational}$  is assumed to follow a similar scaling (without a dependence  $R_{moon}$  of course), with

$$P_{unipolar} \propto \frac{M^{2\gamma} \Omega^{1+2\varepsilon}}{R_{shear}^5}. \quad (17)$$

where  $R_{shear}$  is the radius of the shear zone assumed to terminate the magnetospheric currents in rotational CMI.

As a check, the scaling relationships of Equations 15 and 16 can be applied to the Saturnian moon Enceladus, which is a plasma source within Saturn's magnetosphere (Pontius & Hill 2006), and thus is a potential source of unipolar CMI radiation. Saturn has about 30% of the mass of Jupiter and Enceladus is at an orbital radius of 56% that of Io and has a mean radius only 14% of Io's. The unipolar scaling relations thus predict that Enceladus driven unipolar CMI would only have  $\sim 3 \times 10^{-5}$  of the power of the Io-DAM, or a mean power of  $\sim 4$  MW,  $\sim 0.2\%$  of the total power of the motional driven Saturn Kilometric Radiation (SKR); this scaling thus predicts that the Saturnian-Enceladus unipolar radiation would likely not be separable from the much stronger SKR and in fact it has not yet been observed (Menietti et al. 2007).

There is a large parameter space for unipolar emissions in Equation 15; these parameters are of course unknown for an undiscovered nomadic exoplanet, and, in the complete absence of exomoon data it is unclear what probability distributions would be appropriate for potential exomoons of a hypothetical exoplanet. What is desired is a double power law to scale both  $P_{unipolar}$  and  $P_{motional}$  with the mass and rotational frequency of the primary, when there is, for the mass-power scaling, effectively only a single data point for both the unipolar and rotational cases. In order to proceed, I estimated a unified double power law by assuming that the peak Io-DAM unipolar power and the UCD burst power are typical emissions for their mass and are both subject to the same scaling with mass and rotation frequency, so that the mass scaling can be estimated from the combination of the Io-DAM and UCD data. When the scaling with  $\Omega$  in Equation 16 is applied to the estimates of the radio power for the three UCD sources their spread in power is reduced from a factor of 4.7 to a factor of 1.9, which gives some confidence that this scaling, and the previously determined value for  $\varepsilon$ , applies to rotational as well as unipolar CMI. With these assumptions, the mass scaling exponent is found to be  $\sim 1.38 \pm 0.2$ , or (keeping the formalism of Equation 15)

$$\frac{P_{unipolar/rotational}}{P_{Jupiter}} \sim \left( \frac{R_{moon}}{R_{Io}} \right)^2 \left( \frac{M}{M_{Jupiter}} \right)^{2\gamma-5/3} \left( \frac{\Omega}{\Omega_{Jupiter}} \right)^{1+2\varepsilon} W \quad (18)$$

with the peak  $P_{Jupiter}$  being  $\sim 1.4 \times 10^{12}$  W, the mean being an order of magnitude lower, and the very short duration S-burst flux density being up to  $\sim 7 \times 10^{13}$  W. Equation 18 implies that a “typical” CMI radius scale,  $R_{orbital}$  or  $R_{shear}$  in Equations 16 and 17, is  $\propto M^{1/3}$ ; the  $R_{moon}$  term in Equation 18 should of course be ignored in estimating  $P_{rotational}$ . The model described in Equation 18 is clearly very uncertain, but it does match the very limited available data, and hopefully usefully interpolates the peak power of unipolar and rotational CMI radiation up to  $\sim 80 M_{Jupiter}$ .

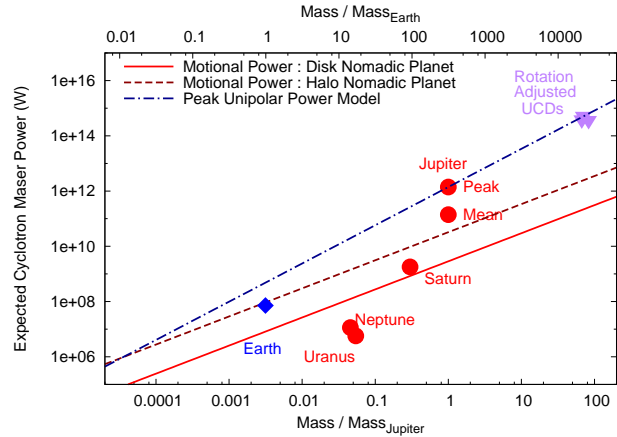


**Figure 12.** The power generated by various models for ISM radiation by nomadic exoplanets, for motional CMI against the ISM (solid and dashed lines, for a disk and a Halo nomad, respectively), together with the unipolar power predicted for an Io-Jupiter analog, respectively, assuming the Jovian rotation period for all masses. The UCD power estimates have been adjusted to the rotation period of Jupiter using the rotation frequency scaling relation of Equation 18

## 6 SEARCHING FOR NOMADIC PLANET RADIO EMISSIONS

Nomadic planet radio emissions at frequencies above the terrestrial ionospheric low-frequency cutoff can be detected by ground-based radio telescope arrays, with the peak flux densities from gas giant nomads likely occurring in the frequency range between 15–200 MHz. The LOw Frequency ARray (LOFAR) (van Haarlem et al. 2013), a large new array specifically intended to observe at those frequencies, is conducting a three-tier sky survey in various channels in the range 15–150 MHz, with “Tier I” being a full survey of the skies visible from Northern Europe, and the Tier II and III surveys consisting of longer integrations restricted to smaller regions of the sky; Table 2 shows the expected sensitivity of these various surveys. The Ukrainian UTR-2 dipole array (Grießmeier, Zarka & Girard 2011) observes in the frequency range 10–32 MHz and has a sensitivity of  $\sim 10$  mJy for a 1 hour integration time, which is a close match to the sensitivity of the LOFAR Tier I survey at 40 MHz. Finally, the Indian Giant Metrewave Radio Telescope, or GMRT (Sirothia et al. 2014) observes at 150 MHz and is conducting the TIFR survey at that frequency with a median flux density limit of 24.8 mJy. The combination of LOFAR, the UTR-2 and the GMRT will be able to constrain or detect Jupiter and super-Jupiter nomadic CMI in the declination range  $90^\circ > \delta \geq -55^\circ$ ; of course, there are a number of other radio telescopes and arrays that can assist in the interpretation of low frequency CMI observations through complementary observations at higher-frequency.

### 6.1 Detecting Nomadic Planet CMI Emissions

CMI sources emit radiation in a fairly narrow cone, and can thus only be seen when this emission cone illuminates the observer. This leads to a periodic emission with a fairly small duty cycle (the fraction of time, typically expressed as

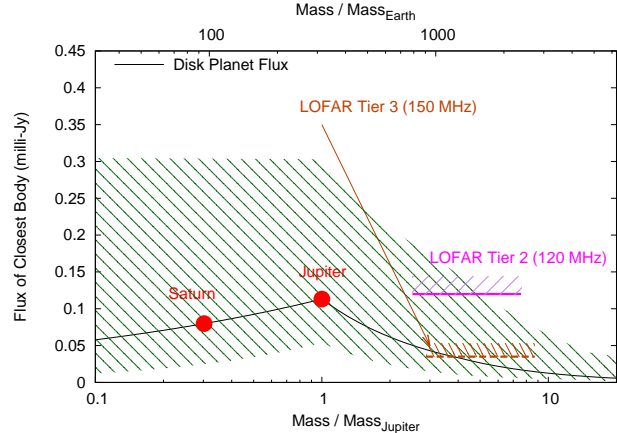
a percentage, in which a source is active). The UCD sources have duty cycles from 5% to 30%, similar to that of Jupiter's 14%; the rapidly rotating UCDs are thus radio loud for some minutes or tens of minutes every 2–3 hr and the Io-flux tube is radio-loud for ~6 hr every 42.5 hr (Nichols et al. 2012). The existence of a CMI duty cycle, plus the variability of emission strength between cycles, implies that a single radio observation of a particular region of the sky would not necessarily detect a nearby nomadic planet in that region; observations will have to be repeated to detect all of the nomadic planet CMI down to the radio flux density limit.

Figure 12 shows the cyclotron power estimates from both the motional and unipolar models, together with rough estimates of the cyclotron maser power emitted by the five magnetic planets in the solar system and the three UCD sources; the UCD source powers shown in this Figure have been adjusted to that expected for a planet of the same mass with the rotation rate of Jupiter using the  $\Omega$  dependence of Equation 18. Two points are shown for Jupiter, corresponding to the mean and peak power; the unipolar model is scaled to fit the peak power. Note that the estimated cyclotron frequency increases rapidly with mass for super-Jupiters (see Figure 12), and thus the total CMI bandwidth also increases rapidly with mass. As the CMI bandwidth increases faster with mass than does the CMI power, the predicted CMI flux density (which depends on the power per Hz, and thus the ratio of the power and the cyclotron frequency) is, for masses larger than Jupiter, predicted to decrease with mass for all three types of CMI emissions.

Figures 13 and 14 show the expected motional flux density from the expected nearest nomadic planet as a function of mass, assuming the entire population is comprised of disk (Figure 13) or Halo (Figure 14) nomadic planets. The factor of ~10 difference in the relative velocity expected for these populations changes the expected flux densities by a similar factor; while the expected motional CMI flux densities from galactic disk nomads would difficult to detect with the planned full-sky LOFAR surveys, or the UTR-2 or GMRT arrays (Figure 13), the LOFAR Tier I survey at 120 MHz would have a reasonable prospect of detecting motion CMI from nearby Halo nomads (Figure 14). Even a failure to detect nomadic planets through motional CMI would bound the number density of Halo nomadic planets; of course, if detected, it should be possible to quickly confirm Halo nomads through their proper motions.

Figure 15 shows the expected unipolar/rotational radio flux density as a function of mass for the closest expected nomadic planets based on Equation 18, together with the various observational limits; the UTR-2 and LOFAR Tier I 40 MHz sensitivities substantially overlap on the scale of this plot. As the LOFAR Tier 1 survey, the GMRT TIRF survey and UTR-2 observations all have a potential for detecting these emissions, and all cover the full sky observable from their locations, the search for unipolar and rotational CMI emissions probably provide the best ground-based means of discovering nearby nomadic exoplanets, at least for bodies with  $M \gtrsim 0.1 M_{Jupiter}$ . (As unipolar CMI seems to be independent of the presence of a host star, the search for these radio emissions could also discover any radio-loud super-Jupiters orbiting the closest stars.)

The flux density predictions shown on Figure 15 are based on the assumption that all nomads of a given mass



**Figure 13.** The motional CMI flux density from the expected nearest nomadic planet of a given mass assuming Equations 9 and 14 and a typical relative velocity for the galactic disk nomad, restricted to masses sufficiently large to probably have a cyclotron frequency above the ionospheric cutoff. The LOFAR flux density limits are for the Tier II and Tier III surveys; none of the LOFAR Tier I surveys would have sufficient sensitivity to likely detect motional CMI from a disk nomad. In this and Figures 14 and 15 the survey limits in MHz are expressed in terms of planetary mass assuming a bandwidth of one half the cyclotron frequency and using the formal errors on the Jupiter-scaling of cyclotron frequencies.

have unipolar or rotational CMI emissions. If, as in the solar system, only one giant nomadic planet in four is capable of unipolar CMI emissions, the expected distance to the nearest such planet would increase by a factor of  $\sqrt[3]{4}$ , and the expected CMI flux density from the nearest radio-loud planet would thus be expected to decrease by a factor of ~2.5; this flux density correction is indicated on Figure 15. The UCD flux densities in Figure 15 are adjusted to the expected minimum distance for brown dwarfs, but not for rotation; the fast rotation frequencies of these bodies substantially increases their flux above the model prediction for the rotation period of Jupiter.

If there is a general tendency for exoplanet rotation rates to increase with mass, as is suggested by rotation rate trend with mass of solar system planets and the only known exoplanet rotation rate, that of  $\beta$  Pictoris b (Snellen et al. 2014), then the closest super-Jupiters with unipolar or rotation CMI are likely to have larger radio flux densities than predicted in Figure 15, and thus be easier to detect with HF radio telescopes. As the Tier I 120 MHz survey should be able to observe the mean unipolar flux density from the closest nomadic Jupiters or super-Jupiters even if these bodies rotate with the same period as Jupiter, and the UTR-2 and the LOFAR 40 and 65 MHz Tier surveys should be able to detect peak emissions from Jupiter mass bodies, there are good prospects of discovering nomadic exoplanet CMI radiation in the 15–120 MHz radio band. The CMI signal to noise ratio could likely be improved, and even more objects discovered, by resolving the time-frequency structure of burst emissions, as discussed in subsection 6.2.

[p]

**Table 2.** Estimated “5  $\sigma$ ” flux density limits for the low frequency channels of the three proposed LOFAR surveys, together with the range of exoplanet masses that would have emissions in each channel, given the “Jupiter-scaling” of cyclotron frequencies (see Figure 11), and the proposed sky coverage for each survey Tier. The UTR-2 telescope survey sensitivity for 10–32 MHz is similar to that of the LOFAR Tier I survey at 40 MHz, while the GMRT TIRF survey at 150 MHz has a mean 5  $\sigma$  sensitivity of  $\sim$ 25 mJy. Note that Jupiter has an upper cyclotron frequency cut-off that is higher than that predicted by its dipole moment, and so it would be visible in a 40 MHz survey.

Frequency	Tier 1 $\sim 2 \pi$ sr	Tier 2 $\sim 0.3$ sr	Tier 3 $\sim 0.025$ sr	$\sim$ Mass Range “Jupiter-Scaling”
MHz	mJy	mJy	mJy	$M_{Jupiter}$
15	60	-	-	0.4 - 1.3
40	10	3.0	-	1.4 - 3.8
65	5	1.2	-	1.8 - 5.1
120	0.8	0.12	-	2.5 - 7.6
150	-	-	0.035	2.9 - 8.8

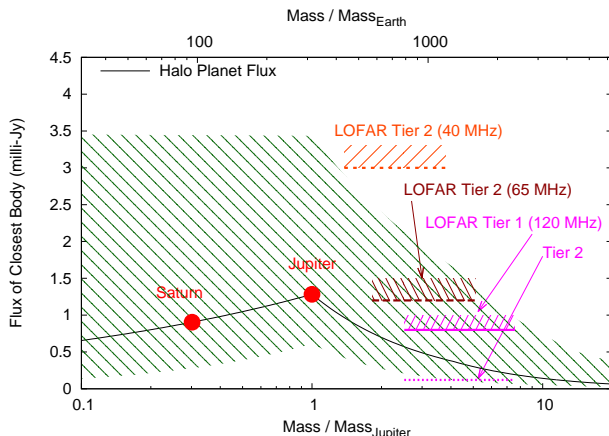


**Figure 14.** The motional CMI flux density from the expected nearest nomadic planet of a given mass assuming Equations 9 and 14 and a typical relative velocity for a galactic Halo object, restricted to masses sufficiently large to probably have a cyclotron frequency above the ionospheric cutoff. The LOFAR flux density limits are for the Tier I and Tier II surveys; the LOFAR Tier I survey at 120 MHz has a good chance of detecting a Halo super Jupiter, assuming that there is a significant population of such objects.

## 6.2 Computational Searches for CMI Radio Emissions

The search for unipolar and rotational CMI radio-frequency emissions from the nearest magnetized planets could be made more sensitive through the application of computational resources. Although CMI radio emissions have a very wide bandwidth when time averaged, in reality at least the Jovian emissions tend to occur in narrow-band bursts of a variety of sorts, with the shortest duration bursts being the S-bursts (Ryabov et al. 2007). These emissions are on a millisecond time scale a very narrow-band signal, with a typical instantaneous bandwidth of a few 100 kHz shifting in frequency at a rate of as much as 18 MHz s $^{-1}$  during the few ms duration of each burst (Ryabov et al. 2007). A matched receiver following this frequency shift would see a much higher flux density, potentially  $\sim$ 1000 times higher than the long term average (this is shown by the upper dashed line in Figure 15). A Jupiter-Io analogue at 3.3 ly would, for example, have a time average flux density at peak of  $\sim$ 10 mJy,

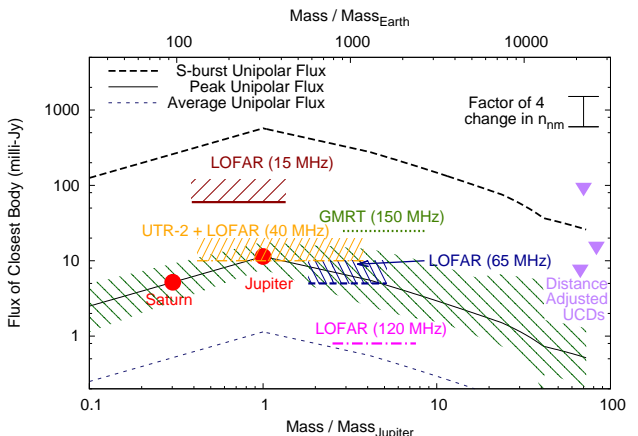


**Figure 15.** The unipolar flux density from the expected nearest nomadic planet of a given mass assuming Equations 9 and 18 and a rotation period equal to that of Jupiter, together with various LOFAR survey flux density limits and the UTR-2 and GMRT flux density limits. Note that the Jupiter point is based on the actual Jovian unipolar flux density, while the Saturn point is purely based on the model and is included as a convenience for the reader only. The UCD flux densities are adjusted for the difference between the actual UCD distance and the expected minimum distance for a brown dwarf (7.26 ly), but are not adjusted for rotation frequency.

which would be marginally detectable by either the UTR-2 or the LOFAR Tier I 40 MHz survey, but it would be 1 Jy or stronger (and thus easily detectable) if the frequency drifts of individual bursts could be followed. A intensive computational effort could be used to improve the signal to noise for nomadic CMI emissions, attempting to detect burst drifts in marginally detected circularly polarized sources (CMI emissions are generally highly circularly polarized) using a wide variety of burst frequency drift and repetition models, in a fashion similar to that employed by SETI@Home (Korpela 2012) in the reduction of possible extraterrestrial communications. This effort would be improved by a more detailed study of the frequency-time structure of the bursts observed from the radio-loud UCDs.

### 6.3 Electrostatic Discharges from Nearby Nomadic Planets

A potential non-CMI source of non-thermal radio emissions from nearby nomadic exoplanets are emissions caused by electrostatic discharges from planetary lightning. The Voyager and Cassini spacecraft detected lightning-related radio emissions from Saturn, the so-called Saturn Electrostatic Discharges (SED), which have since been observed on the ground by the UTR-2 array (Grießmeier, Zarka & Girard 2011; Grießmeier et al. 2011). (The radiation from electrostatic discharges on Jupiter is apparently trapped by the Jovian ionosphere, and is not observable from a distance.) The SED are a broad spectrum source up to a limiting frequency of  $\sim 20$  MHz, consisting of bursts with a typical duration of order 0.1 s occurring in “episodes” lasting a few hours, with each SED burst having a typical flux density density of order 1 Jy when observed from Earth at a distance of  $\sim 10$  AU. While typical SED bursts would have a very small flux density at 2.68 ly (the expected distance for a Saturn mass nomadic exoplanet), the peak SED burst intensity is  $\sim 1000$  Jy at 10 AU, equivalent to  $\sim 4 \mu\text{Jy}$  at 2.68 ly, too weak to detect with current surveys, but possibly within reach of a dedicated instrument. Lightning events on Earth can produce X-rays and gamma rays with energies up to  $\sim 2$  MeV, and of course also produce visible light, all of which could be conceivably detected across a few light years. If a nearby nomadic exoplanet were to be discovered by other means, electrostatic discharges would be a logical target for follow-up observations; Bailey et al. (2014) describe various instruments suitable for detecting nearby exoplanet electrostatic discharges across a wide range of energies.

## 7 GRAVITATIONAL LENSING OF NEARBY NOMADIC PLANETS

At present, most exoplanets have been detected either by radial velocity (Doppler) measurements, or by surveys searching for either stellar transits or gravitational microlensing events. While stellar Doppler and orbital transit events are not suitable for detecting nomadic planets, there is some chance of detecting nearby nomadic planets with microlensing. Unfortunately, the optical depths of gravitational lensing of neighboring nomadic planets are sufficiently low that the detection of significant numbers of nearby nomads by ground based microlensing surveys is unlikely. The integrated optical depth for a lensing event by a single close nomadic planet of  $\sim M_{\text{Jupiter}}$  would be about  $10^{-14}$  per year, with event duration being of order 1 hour. As there are unlikely to be more than a few hundred Jupiters and super-Jupiters within the detection range of (say) SPICA or JWST (see Table 1), the detection of one such close nomad in a decade would require continual monitoring of order  $10^{11}$  stars. The optical depth is a little more favorable for astrometric mesolensing, with an integrated optical depth of  $\sim 3 \times 10^{-12}$  per year for a 20  $\mu\text{as}$  astrometric perturbation of a background star, with such an event lasting on order 2 weeks. As one billion stars is the projected size of the Gaia telescope catalog (Lindegren 2010), it is just possible that Gaia would observe such an astrometric mesolensing event over a 5 year mission lifetime (Belokurov & Evans 2002;

Gaudi & Bloom 2005). It however seems unlikely that there will be significant numbers of neighboring nomadic planets discovered by microlensing or mesolensing until there are space telescopes dedicated to deep, high-cadence, microlensing or mesolensing surveys.

Neighboring nomadic planets, once discovered, will however be good candidates for predicted microlensing observations (Paczynski 1995). A nearby nomad will be rapidly moving across the sky (a Jupiter-mass body at 3.3 ly and a transverse velocity of  $30 \text{ km s}^{-1}$  would have an angular velocity of  $\sim 6 \text{ arc sec yr}^{-1}$ ); once discovered, it should be possible to search for stars in the future path of a nomad and thereby predict and observe upcoming gravitational lensing events, with a goal of directly measuring the planetary mass and detecting or bounding any companions. Such events have already been predicted, and should be observed for Proxima Centauri (Sahu et al. 2014), for the same purposes.

For lensing by distant objects (say in the galactic bulge), it is not generally possible to separate the lens and source images, and so for point mass lensing the lens mass, distance and transverse motion are all unknown, leading to degeneracies in the determination of the lens mass. In the case of lensing by a nearby object, the lens distance and transverse velocity can be determined directly from pre and post-event astrometry, and thus a single microlensing event could directly determine the mass of the lens (Sahu et al. 2014). A further advantage for predictive nomadic planet lensing is that the lens (the nomadic planet) would have basically no optical emissions and thus would not overwhelm the photometry and astrometry of the background source, as can happen with close star lensing. This would make it possible to observe lensing events with very faint sources, increasing the probability finding an upcoming event. Finally, the Einstein radii of nomadic planet lenses within 5 or 10 ly of the solar system are small enough that in many cases the terrestrial parallax (Gould et al. 2009) between observatories would be significant, and this could also help break lens degeneracies and improve the detectability of lens companions (Gould & Yee 2013).

## 8 ASTROBIOLOGY AND THE NEARBY NOMADIC PLANETS

Neighboring nomads will, through planetary migration, provide a sampling of the biological potential (or development) of the galaxy. Terrestrial nomads, either as primaries or as moons of giant nomads, would undoubtedly have very cold exteriors (see Figure 5), but that does not mean that they could not be inhabitable (in an astrobiological sense), potentially supporting active biospheres without being within any stellar habitable zone (Stevenson 1999; Abbot & Switzer 2011; Badescu 2011). Nomad inhabitability would require insulation of a habitable region from the vacuum and heat loss of deep space, and also sources of internal heating, such as by radionuclides or, in the case of exomoons, by tidal heating.

Nomadic planets could thus have “insulated” biospheres evolving under nomadic conditions with no stellar heat input. Stevenson (1999) proposed that 1 Earth-mass planets could have surface oceans of liquid water, and thus conceivably biologies, insulated by thick Hydrogen-Helium (H-He)

atmospheres with pressure induced far-IR opacity. The subsequent discovery that for  $M \gtrsim 4 M_{Earth}$  terrestrial planet radii are roughly  $\propto$  mass strongly suggests that H-He atmospheres are common for at least these super-Earths (Marcy et al. 2014; Wu & Lithwick 2013); surface water oceans may thus be possible for some super-Earth nomads. Abbot & Switzer (2011) have suggested that nomadic “Steppenwolf” planets, with  $M \gtrsim 3.5 M_{Earth}$ , could have internal liquid water oceans insulated by a thick shell of water (and possibly other) ices. There are of course a number of possible examples in the solar system of insulated internal hydrospheres warmed by tidal heating, with candidates currently including Europa, Callisto, Ganymede, Enceladus, Titan and Triton (Hussmann, Sohl & Spohn 2006); there is no reason not to expect similar sub-surface oceans on nomad exomoons (Ehrenreich & Cassan 2007).

Stellar nomadic planets could also have “fossil” biospheres, the remnants of any biospheres evolving before they were ejected from their stellar system. These could be dead, or the ejected planet biosphere could have subsequently evolved to survive in an insulated ocean, in deep rock formations, or in other insulated regions. These various possibilities thus suggest that the nearest exobiologies could well exist on a yet-to-be-found nearby nomadic planet. It is even possible that nomadic planets ejected sufficiently long after their formation could host remains of technological civilizations. The exploration of nomadic planets thus has the potential of significantly constraining the probability and nature of biologies arising in the galaxy and (should post-formation ejection be common) also the probability of technical civilizations arising in stellar systems in the galaxy.

## 9 CONCLUSIONS

I have shown in this paper that nomadic exoplanets should be found closer than the nearest stars, that these close nomads will sample the galactic history of planetary formation and evolution, and that, while terrestrial nomads will probably be out of reach of the current generation of astronomical instruments, the closest Saturn, Jupiter and super-Jupiter nomads should be discoverable by either their far-IR thermal emission, or by their radio CMI emissions in the 15–120 MHz HF band. Once detected, the neighboring nomadic exoplanets should become a fruitful area of astronomical research; although dim in optical wavelengths, their IR and radio emissions would not be overwhelmed by radiation from a stellar primary, and their closeness would allow detailed astronomical study, for example by the determination of masses through predictive microlensing or by the detection of their electrostatic emissions. Once found, the close nomadic exoplanets should be of astrobiological interest, with a possibility of both fossil biospheres (for planets ejected from stellar systems), and active insulated biospheres (for both ejected and native nomads). In the longer run, as both the closest exoplanets and as possible locations of biospheres, the neighboring nomadic planets are likely to become the initial targets for interstellar exploration by spacecraft.

## ACKNOWLEDGMENTS

This work was sponsored by Asteroid Initiatives LLC and by Stephanie Eubanks. I am grateful to Bruce Bills and to Adam Crowl for comments and discussions.

## REFERENCES

- Abbot D. S., Switzer E. R., 2011, *Ap. J. Lett.*, 735, L27
- Alcock C. et al., 1998, *Ap. J. Lett.*, 499, L9
- Badescu V., 2011, *Icarus*, 216, 485
- Bailey R. L., Helling C., Hodosán G., Bilger C., Stark C. R., 2014, *Ap. J.*, 784, 43
- Barlow M. J., 2012, in IAU Symposium, Vol. 283, IAU Symposium, pp. 295–301
- Baudry A., 2008, in 2nd MCCT-SKADS Training School. Radio Astronomy: Fundamentals and the New Instruments
- Beaulieu J.-P., Tisserand P., Batista V., 2013, in European Physical Journal Web of Conferences, Vol. 47, European Physical Journal Web of Conferences, p. 15001
- Belokurov V. A., Evans N. W., 2002, *Mon. Not. R.A.S.*, 331, 649
- Bose S. K., Sarkar S., Bhattacharyya A. B., 2008, *Indian Journal of Radio and Space Physics*, 37, 77
- Bovy J., Tremaine S., 2012, *Ap. J.*, 756, 89
- Cecconi B. et al., 2012, *Planet. Space Sci.*, 61, 32
- Chabrier G., 2001, *Ap. J.*, 554, 1274
- Chabrier G., Baraffe I., Leconte J., Gallardo J., Barman T., 2009, in American Institute of Physics Conference Series, Vol. 1094, 15th Cambridge Workshop on Cool Stars, Stellar Systems, and the Sun, Stempels E., ed., pp. 102–111
- Cieplak A. M., Griest K., 2013, *Ap. J.*, 767, 145
- Davies J. H., Davies D. R., 2010, *Solid Earth*, 1, 5
- del Peloso E. F., da Silva L., Porto de Mello G. F., Arany-Prado L. I., 2005, *Astron. Astrophys.*, 440, 1153
- Delorme P. et al., 2012, *Astron. Astrophys.*, 548, A26
- Doyle J. G., Antonova A., Marsh M. S., Hallinan G., Yu S., Golden A., 2010, *Astron. Astrophys.*, 524, A15
- Durand-Manterola H. J., 2009, *Planetary and Space Science*, 57, 1405
- Ehrenreich D., Cassan A., 2007, *Astronomische Nachrichten*, 328, 789
- Fogg M. J., 1990, *Comments on Astrophysics*, 14, 357
- Fortney J. J., Ikoma M., Nettelmann N., Guillot T., Marley M. S., 2011, *Ap. J.*, 729, 32
- Gaudi B. S., Bloom J. S., 2005, *Ap. J.*, 635, 711
- Gould A. et al., 2009, *Ap. J. Lett.*, 698, L147
- Gould A., Yee J. C., 2013, *Ap. J.*, 764, 107
- Grießmeier J.-M., Zarka P., Girard J. N., 2011, *Radio Science*, 46, 0
- Grießmeier J.-M. et al., 2011, *Planetary, Solar and Heliospheric Radio Emissions (PRE VII)*, 145
- Griest K., Cieplak A. M., Lehner M. J., 2013, *Phys. Rev. Lett.*, 111, 181302
- Hallinan G., Antonova A., Doyle J. G., Bourke S., Lane C., Golden A., 2008, *Ap. J.*, 684, 644
- Hanel R. A., Conrath B. J., Kunde V. G., Pearl J. C., Pirraglia J. A., 1983, *Icarus*, 53, 262
- Hatzes A. P., 2014, *Nature*, 513, 353

- Howard A. W. et al., 2014, *Ap. J.*, 794, 51
- Hussmann H., Sohl F., Spohn T., 2006, *Icarus*, 185, 258
- Jester S., Falcke H., 2009, *New Astronomy Reviews*, 53, 1
- Jung Y. K., Park H., Han C., Hwang K.-H., Shin I.-G., Choi J.-Y., 2014, *Ap. J.*, 786, 85
- Kirkpatrick J. D. et al., 2012, *Ap. J.*, 753, 156
- Korpela E. J., 2012, *Annual Review of Earth and Planetary Sciences*, 40, 69
- Lazio, W. T. J., Farrell W. M., Dietrick J., Greenlees E., Hogan E., Jones C., Hennig L. A., 2004, *Ap. J.*, 612, 511
- Li L. et al., 2012, *J. Geophys. Res. (Planets)*, 117, 11002
- Li L. et al., 2010, *J. Geophys. Res. (Planets)*, 115, 11002
- Lindegren L., 2010, in *IAU Symposium*, Vol. 261, *IAU Symposium*, Klioner S. A., Seidelmann P. K., Soffel M. H., eds., pp. 296–305
- Lissauer J. J., Dawson R. I., Tremaine S., 2014, *Nature*, 513, 336
- Luhman K. L., 2013, *Ap. J. Lett.*, 767, L1
- Luhman K. L., 2014a, *Ap. J.*, 781, 4
- Luhman K. L., 2014b, *Ap. J. Lett.*, 786, L18
- Luhman K. L., Esplin T. L., 2014, ArXiv e-prints
- Marcy G. W., Weiss L. M., Petigura E. A., Isaacson H., Howard A. W., Buchhave L. A., 2014, ArXiv e-prints
- Mayor M., Lovis C., Santos N. C., 2014, *Nature*, 513, 328
- Menietti J. D., Groene J. B., Averkamp T. F., Hospodarsky G. B., Kurth W. S., Gurnett D. A., Zarka P., 2007, *Journal of Geophysical Research (Space Physics)*, 112, 8211
- Mordasini C., Alibert Y., Georgy C., Dittkrist K.-M., Klahr H., Henning T., 2012, *Astron. Astrophys.*, 547, A112
- Nesti F., Salucci P., 2013, *J. Cosmology and Astroparticle Physics*, 7, 16
- Nichols J. D., Burleigh M. R., Casewell S. L., Cowley S. W. H., Wynn G. A., Clarke J. T., West A. A., 2012, *Ap. J.*, 760, 59
- Onaka T. et al., 2004, in *ESA Special Publication*, Vol. 554, 5th International Conference on Space Optics, Warmbein B., ed., pp. 297–302
- Öpik E. J., 1964, *Irish Astronomical Journal*, 6, 290
- Paczynski B., 1995, *Acta Astronomica*, 45, 345
- Pearl J. C., Conrath B. J., 1991, *J. Geophys. Res.*, 96, 18921
- Pearl J. C., Conrath B. J., Hanel R. A., Pirraglia J. A., 1990, *Icarus*, 84, 12
- Pontius D. H., Hill T. W., 2006, *Journal of Geophysical Research (Space Physics)*, 111, 9214
- Roškar R., 2013, *Memorie della Societa Astronomica Italiana Supplementi*, 25, 64
- Ryabov V. B., Ryabov B. P., Vavrik D. M., Zarka P., Kozhin R., Vinogradov V. V., Shevchenko V. A., 2007, *J. Geophys. Res. (Space Physics)*, 112, 9206
- Sahu K. C., Bond H. E., Anderson J., Dominik M., 2014, *Ap. J.*, 782, 89
- Schneider J., Dedieu C., Le Sidaner P., Savalle R., Zolotukhin I., 2011, *Astron. Astrophys.*, 532, A79
- Siegler M. A., Smrekar S. E., 2014, *J. Geophys. Res. (Planets)*, 119, 47
- Sirothia S. K., Lecavelier des Etangs A., Gopal-Krishna, Kantharia N. G., Ishwar-Chandra C. H., 2014, *Astron. Astrophys.*, 562, A108
- Snellen I. A. G., Brandl B. R., de Kok R. J., Brogi M., Birkby J., Schwarz H., 2014, *Nature*, 509, 63
- Stevenson D. J., 1999, *Nature*, 400, 32
- Stier M. T., Traub W. A., Wright E. L., Low F. J., 1978, *Ap. J.*, 226, 347
- Strigari L. E., Barnabè M., Marshall P. J., Blandford R. D., 2012, *Mon. Not. R.A.S.*, 423, 1856
- Sumi T. et al., 2011, *Nature*, 473, 349
- van Haarlem M. P. et al., 2013, *Astron. Astrophys.*, 556, A2
- Vanhamäki H., 2011, *Planet. Space Sci.*, 59, 862
- Veras D., Mustill A. J., Bonsor A., Wyatt M. C., 2013, *Mon. Not. R.A.S.*, 431, 1686
- Veras D., Raymond S. N., 2012, *Mon. Not. R.A.S.*, 421, L117
- Vican L., 2012, *Astron. J.*, 143, 135
- Wright E. L. et al., 2010, *Astron. J.*, 140, 1868
- Wu Y., Lithwick Y., 2013, *Ap. J.*, 772, 74
- Zapatero Osorio M. R., Béjar V. J. S., Martín E. L., Rebolo R., Barrado y Navascués D., Bailer-Jones C. A. L., Mundt R., 2000, *Science*, 290, 103
- Zarka P., 1998, *J. Geophys. Res.*, 103, 20159
- Zarka P., 2010, in *Astronomical Society of the Pacific Conference Series*, Vol. 430, *Pathways Towards Habitable Planets*, Coudé du Foresto V., Gelino D. M., Ribas I., eds., p. 175

This paper has been typeset from a TeX/ L<sup>A</sup>T<sub>E</sub>X file prepared by the author.